SSRG International Journal of Electronics and Communication Engineering
ISSN: 2348-8549/ https://doi.org/10.14445/23488549/IJECE-V13I7P122

Volume 13 Issue 7, 311-322, July 2026

Original Article

Hysteresis-Based Switching Design for Hybrid FSO-RF System using OptiSystem-MATLAB Co-Simulation

Shirley Musima[1], Kibet Langat[2], Nicholas Oyie[3]

[1]*Electrical Engineering Department, Pan African University Institute of Basic Sciences, Technology and Innovation, Juja, Kenya*
[2]*Department of Telecommunications & Information Engineering, Jomo Kenyatta University of Science and Technology, Juja, Kenya*
[3]*School of Engineering and Technology, Murang'a University of Technology, Murang'a, Kenya*

[1]*Corresponding Author : nangami.shirley@students.jkuat.ac.ke*

Received: 17 March 2026 Revised: 21 April 2026 Accepted: 19 June 2026 Published: 29 July 2026

Abstract - *Hybrid FSO-RF communication systems improve link availability in high-capacity 5G-and-beyond wireless backhaul. However, practical deployment strongly depends on the choice of switching mechanism and the selection of suitable thresholds under varying atmospheric conditions. This paper implements a joint OptiSystem-MATLAB co-simulation framework for evaluating hysteresis-based switching in a hybrid FSO-RF system under the combined effects of atmospheric turbulence, fog and rainfall. The framework is used to assess outage performance and switching stability relative to conventional hard-switching approaches. Simulation results indicate an overall reduction of 99.49% in the outage fraction relative to the FSO-only link across the evaluated visibility conditions, while all the links maintain zero outage under the rainfall conditions considered. Additionally, the hysteresis-based switching reduces switching events by 22% relative to a single threshold switch while maintaining low outage probability. The obtained results quantify the impact of threshold selection on outage probability and switching rate under turbulence, fog and rainfall conditions.*

Keywords - *Atmospheric turbulence, Free-Space Optics, Hysteresis, Signal-To-Noise Ratio, Weather attenuation.*

1. Introduction

The push toward 5G-and-beyond wireless infrastructure has placed unprecedented throughput demands on backhaul networks. Traditional microwave networks face limitations due to scarce spectrum and susceptibility to adverse atmospheric conditions. Optical fiber, on the other hand, offers high capacity and reliability but presents costly deployment and logistical challenges in remote areas or dense urban environments. Consequently, alternative wireless backhaul technologies are highly sought after.

Millimeter wave technology offers unlimited spectrum, high speeds with minimal latency and compact antenna-array implementation [1, 2]. However, it suffers from oxygen absorption and severe atmospheric attenuation in rainy conditions. Although techniques such as massive MIMO [3], beamforming and ultra-cell densification can improve performance, they often increase system complexity and hardware cost. Free Space Optics (FSO) is another complementary technology that offers a license-free spectrum, high security and high transmission speeds (up to 15Gbps) and requires minimal initial investment [4]. However, its performance is strongly affected by fog, rain, snow, haze, atmospheric turbulence and pointing errors. In addition, it has a smaller coverage area and requires a strict Line Of Sight (LOS) for its transmission. Since the two technologies are affected differently by atmospheric conditions, a hybrid system comprising the two technologies allows them to complement each other and improve overall link availability and reliability.

A primary challenge in hybrid system architecture [4] is the design of an effective network selection mechanism that ensures seamless transmission of data without unnecessary switching oscillations. In practice, the effectiveness of this decision relies not only on the switching rule itself but also on the thresholds triggering switching. For hybrid FSO-RF systems, threshold selection can be challenging because link quality can be affected by atmospheric turbulence, weather-induced attenuation and/or pointing errors.

2. Related Works

Switching mechanisms are grouped into either hard or soft switching. Previous studies into soft switching mechanisms have utilized techniques such as Raptor codes [5], Fuzzy Logic Inference Systems (FIS) [6], and Low-

Density Parity Check (LDPC) codes [7]. In [6], the effects of both atmospheric turbulence and fog-induced attenuation are studied, while in [8], switching of a hybrid FSO-RF system using a fog sensor is analyzed, but the impact of atmospheric turbulence is not considered in the analysis. In hard switching, researchers have largely focused on threshold design. Impairment-specific switching behavior has also been the focus of several studies. In [9], switching is considered during atmospheric turbulence only, but the procedure used to select the thresholds for switching is not discussed concisely. In [10], the authors investigate the effect of hard switching using power and time hysteresis algorithms, but only consider the effects of weak turbulence and pointing errors.

The work in [11] demonstrated the significance of level crossing rate when studying outage performance using a single threshold only for switching, and in [12, 13], both works considered single and dual thresholds, but all of them considered only the effects of atmospheric turbulence. Pointing errors in FSO links are extensively discussed in [14], while [15] presents a dual threshold hybrid system that examines the effects of atmospheric turbulence and pointing error only. While existing literature explores specific, isolated impairments, there is a distinct lack of comprehensive co-simulation testbeds capable of validating hard-switching thresholds across combined, realistic atmospheric conditions. This gap is addressed in this paper by presenting a joint MATLAB–OptiSystem co-simulation framework that evaluates a hysteresis-based hard switching mechanism under the simultaneous effects of atmospheric turbulence, fog and rainfall. Compared with single-threshold and FIS-based approaches, the proposed method reduces switching events by 22% while maintaining near-zero outage probability.

Machine learning and deep reinforcement learning have also been used for hybrid FSO-RF switching, with the aim of predicting link degradation and enabling more adaptive switching decisions. Techniques reported in the literature include decision trees [16, 17], recurrent neural networks [18-20], artificial [21] neural networks, use of fuzzy logic [6], Gaussian Process Classifier [22], camera-based perception method [23], Random Forest [24] and DQNEnsemble consensus representation [25] In this context, the fixed thresholds obtained in this work serve as a useful baseline for future intelligent and adaptive switching algorithms based on deep reinforcement learning.

The rest of this paper is structured as follows. Section 2 presents the system design and channel models, Section 3 details the performance analysis, Section 4 discusses the results, and Section 5 concludes the paper.

3. System Architecture

3.1. FSO System

The FSO channel is based on Intensity Modulation (IM)/Direct Detection (DD), On-Off (OOK) modulation technique. Space diversity (4*4 MIMO) technology is employed to combat fading caused by atmospheric turbulence and atmospheric weather conditions. NRZ-OOK is selected as the modulation scheme due to its widespread adoption in commercial FSO deployments where receiver complexity is kept low. For this work, geometrical losses, losses due to attenuation and scintillation are considered. Geometrical loss is caused by the spreading of the transmitted beam between the transmitter and the receiver. Pointing error-induced fading is considered sufficiently small to be excluded in this setup, given the short link distance, rigid transceiver mounting and accurate beam alignment. An Erbium-Doped Fiber Amplifier (EDFA) is used on the receiver end to maximize the gains achieved. EDFA tends to exhibit lower noise levels and higher gain and is suited for long-distance and high-performance telecommunication systems. The optical power received, P_R is calculated using the formula in equation 1 [26]:

$$P_r = P_t \left(\frac{D_r}{D_t + \theta_{div} L}\right)^2 \eta_T \eta_R G h \quad (1)$$

Where P_t is the transmitted power in watts, D_t (m) is the transmitter aperture diameter, D_r (m) is the receiver aperture diameter, θ_{div} (mrad) is the full transmitting divergence angle, L(km) is the link distance, η_T, η_R are the optical efficiencies of the transmitter and receiver, respectively, *L(km)* is the link length, G is the gains due to EDFA, and *h* is the channel state.

The channel state will be represented as:

$$h = h_a h_t \quad (2)$$

Atmospheric attenuation, h_a is modelled by Beer-Lambert's law as [26]:

$$h_a = \exp(-\alpha . L) \quad (3)$$

Where $\alpha(\lambda) \cong \frac{3.91}{V} (\frac{\lambda}{550})^{-q}$; v is visibility in km, and λ is wavelength in nm.

The value of q as per Kim's model is given by [20]:

$$q = \begin{cases} 1.6, & V > 50\text{km} \\ 1.3, & 6\text{km} < V < 50\text{km} \\ 0.16V + 0.34, & 1\text{km} < V < 6\text{km} \\ V - 0{,}5, & 0.5\text{km} < V < 1\text{km} \\ 0, & V < 0.5\text{km} \end{cases} \quad (4)$$

Using the international visibility code in [27], the attenuation values for diverse weather conditions are obtained using equations 3 and 4 and are tabulated in Table 1. To characterize how rainfall affects the FSO link specifically, the power-law attenuation model $\alpha = k_1 R^{k_2}$ is used where R is the rain rate and k_1 = 0.509 and k_2 = 0.63 are parameters provided for in [28].

Atmospheric turbulence is modelled after the gamma-gamma distribution fading model that considers moderate to strong turbulent conditions. In a MIMO FSO system employing spatial diversity, the turbulence-induced channel gain between the i-th transmit aperture and the j-th receive aperture is expressed as

$$h_t = h_{ij} = X_{ij} \cdot Y_{ij} \quad (5)$$

Where X_{ij} and Y_{ij} are statistically independent components following a Gamma distribution: $X_{ij} \sim \Gamma(\alpha, 1/\alpha)$ and $Y_{ij} \sim \Gamma(\beta, 1/\beta)$ respectively. α governs large-scale irradiance variations driven by cells of atmospheric turbulence, while β captures small-scale scintillation at the receiver aperture.

$$\alpha = \left[exp\left(\frac{0.49\sigma^2{}_R}{\left(1+1.11\sigma^{\frac{12}{5}}{}_R\right)^{\frac{7}{6}}} \right) - 1 \right]^{-1} \quad (6)$$

$$\beta = \left[exp\left(\frac{0.51\sigma^2{}_R}{\left(1+0.69\sigma^{\frac{12}{5}}{}_R\right)^{\frac{5}{6}}} \right) - 1 \right]^{-1} \quad (7)$$

Where $\sigma_R = 0.5C^2{}_n k^{7/6} L^{11/6}$ It is Rytov variance, which is also an indicator of turbulence strength and is approximately equal to the scintillation index in weak turbulence. C_n^2 is the refractive index parameter, $k = 2\pi/\lambda$ is the wave number, and λ denotes the wavelength.

The effective channel state is obtained through equal gain combining of all channel states, and the composite channel gain is obtained by summing the individual branch gains across all transmit–receive aperture pairs, yielding

$$h_t = \sum_i^{N_t} \sum_j^{N_r} h_{ij} \text{q} \quad (8)$$

In the considered FSO configuration of four transmit and four receiver antennas, this corresponds to a diversity order of $N_t N_r = 16$, providing improved robustness against turbulence-induced fading.

The parameters that were used in the design of the FSO and RF system model are shown in Tables 2 and 3, respectively.

3.2. MM-Wave RF System

The mm-wave RF channel is modeled as a Rician fading model to characterize propagation conditions with a dominant line-of-sight component, which is characteristic of FSO links and is appropriate for backhaul scenarios. This assumption does not fully capture severe blockage or multipath environments where the LOS component may be intermittently obstructed. 16- Quadrature Amplitude Modulation (QAM) scheme is used to mitigate channel-induced impairments. The RF received signal is expressed as:

$$r = \sqrt{h_l}\, h_a e + n \quad (9)$$

Where n is AWGN; h_l is the fading coefficient; e is the transmitted signal, and h_a is the RF link path loss.
The RF link path loss can be expressed as

$$h_a = \frac{G_T G_R}{({}^{4\pi L}/_{\lambda})^2 \alpha_{rain} \alpha_{oxy} L} \quad (10)$$

Where G_T, G_R is the gain of the transmitter and receiver, respectively, $({}^{4\pi L}/_{\lambda})^2$ is the free space path loss, L is the link distance in km, and $\alpha_{rain,}\alpha_{oxy}$ is the attenuation due to rainfall and oxygen, respectively. Attenuation due to rainfall as per the guidelines in ITU 530.18 is specified as $\alpha = S_R L_{eff} = S_R Lr$ dB where S_R is specific attenuation per km, and L_{eff} is the effective path length. S_R can be calculated using the guidelines provided in ITU-R P.838 as: $S_R = aR^b$ dB/km where a and b give the regression factors that are dependent on several aspects such as the temperature, distribution of rain drop size, frequency and polarization, and R is the rain rate.

The PDF for a Rician channel can be expressed as [29]:

$$f_{RF}(h_{a1}) = 2(k+1)h_{a1}\left(-k-(k+1){h_{a1}}^2\right) * I_0(2h_{a1}\sqrt{k(k+1)} \quad (11)$$

3.3. MATLAB–OptiSystem Co-Simulation Architecture

OptiSystem 22 and MATLAB R2024b are integrated to implement a co-simulation framework for a hybrid FSO-RF communication system.

OptiSystem is used to model the physical-layer components for both the FSO and RF links and to evaluate link performance at the component level. Since OptiSystem does not provide native mmWave RF propagation models, the RF channel, including Rician fading, is modeled in MATLAB and linked to the OptiSystem design through the MATLAB component. The MATLAB component allows external MATLAB code to be included within the communication system simulation.

The overall hybrid FSO–RF system configuration used in this work is shown in Figure 1. The switching process is controlled by an independent MATLAB script implementing the hysteresis-based decision algorithm.

At the start of each simulation run, the script initializes the OptiSystem project file, applies the relevant atmospheric and channel parameters, and extracts the average SNR values for both links at the end of each OptiSystem run. These SNR values are compared with the predefined switching thresholds to determine the active transmission link. A quasi-static channel assumption is adopted, where atmospheric conditions remain constant during one simulation run. Therefore, the switching decisions are made between consecutive simulation runs corresponding to different channel states, rather than during a single simulation window. The co-simulation architecture is shown in Figure 2.

Table 1. Attenuation values for the FSO link based on Kim's model for a 1km link range

Weather condition	Visibility (m)	Attenuation [dB/KM]
Thick fog	200	84.9
Moderate fog	500	33.96
Light fog/Storm (100 mm/h)	770 – 1000	19.72 – 10.12
Thin fog/heavy rain (25 mm/h)	1900 – 2000	4.59 – 4.29
Haze/medium rain (12.5 mm/h)	2800 – 4,000	2.69 – 0.11
Clear air /drizzle (0.25 mm/h)	18000 – 20,000	0.245 – 0.22
Very clear air	23,000 – 50,000	0.19 – 0.065

Table 2. FSO link parameters

Parameter	Value
Wavelength, λ	1550 nm
Transmission power, Tx	0 dBm
Data rate	10 Gbps
Transmitter and receiver efficiency, η_T, η_R	1
Transmitter aperture diameter, W	5 cm
Beam divergence, θ	2 mrad
Link range, L	1 km
Index refraction structure for moderate turbulence, C_n^2	10^{-14} $m^{-2/3}$
Receiver aperture diameter, D_R	20 cm
Responsivity of diode, R	0.9 A/W
Modulation scheme	NRZ-OOK

3.4. Hysteresis-based Switching Mechanism

Conventional hard-switching schemes rely on instantaneous threshold-based decisions, which can lead to frequent and undesirable link oscillations (ping-pong effect) under rapid random fluctuations of the received signal.

To mitigate this behavior, power and time hysteresis methods are effective in avoiding unnecessary frequent switching [9, 12, 13].

Link selection in this setup is governed by the average SNR value measured at the receiver front-end.

Specifically, the SNR of the RF and FSO links are obtained using the Electrical Carrier Analyzer (ECAN) and WDM Analyzer for the RF and FSO link, respectively and fed back to the external control (MATLAB), where it is compared against predefined SNR switching thresholds incorporating hysteresis margins. A combined power-hysteresis and persistence hold mechanism is employed, whereby a link switch is triggered only after sustained violation of the SNR threshold over 3 consecutive observation intervals.

The switching logic is summarized in the flowchart shown in Figure 3.

To demonstrate the complementary nature of the FSO and RF links in combating atmospheric impairments, both links are continuously evaluated within the simulation framework, while only the selected link contributes to the output performance metrics.

Table 3. Mm wave RF link parameters

Parameter	Value
Frequency	60 GHz
Link range	1 km
Transmitter antenna gain, G_T	16 dBi
Receiver antenna gain, G_R	30 dBi
Rice factor, K	8
Frequency-dependent coefficient, b	0.7656
Attenuation constant at 60Ghz (horizontal polarization), a	0.8606
Rain rate, $R_{0.01}$	0 - 100 mm/h
Oxygen attenuation, α_{oxy}	14.79 dB
Bit rate, b/s	10^9
Modulation scheme	16-QAM

The integrated co-simulation framework enables realistic modeling of channel dynamics while supporting dynamic switching between the FSO and RF links.

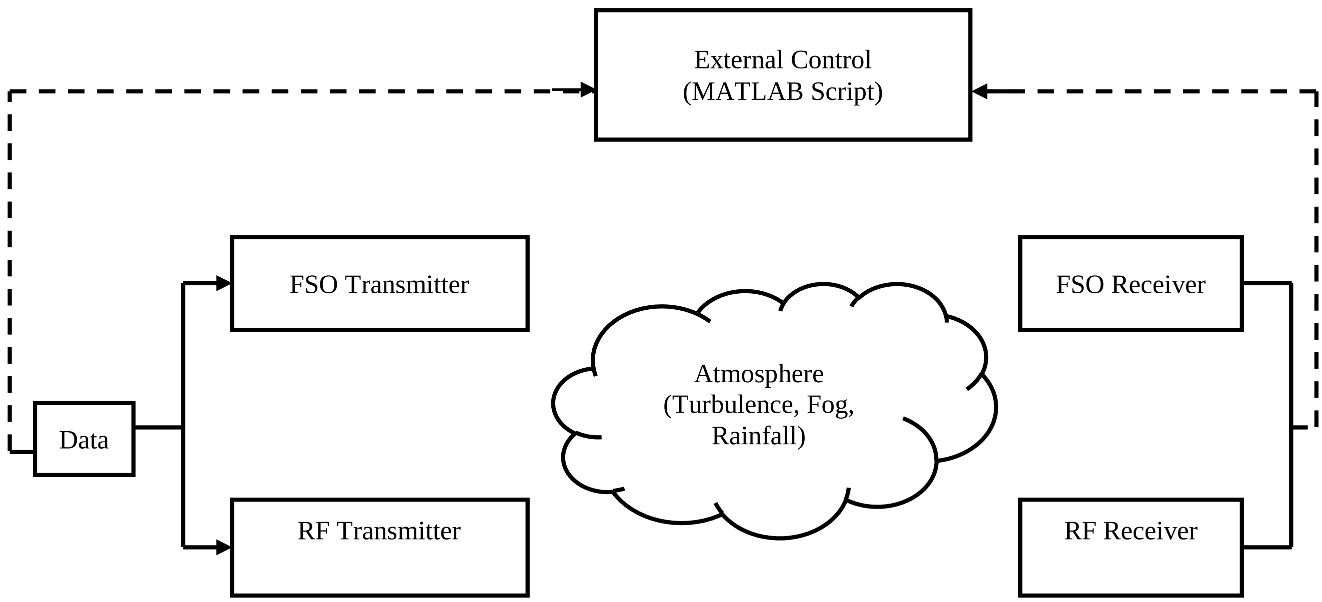

Fig. 1 Block diagram of the hybrid FSO-RF communication system

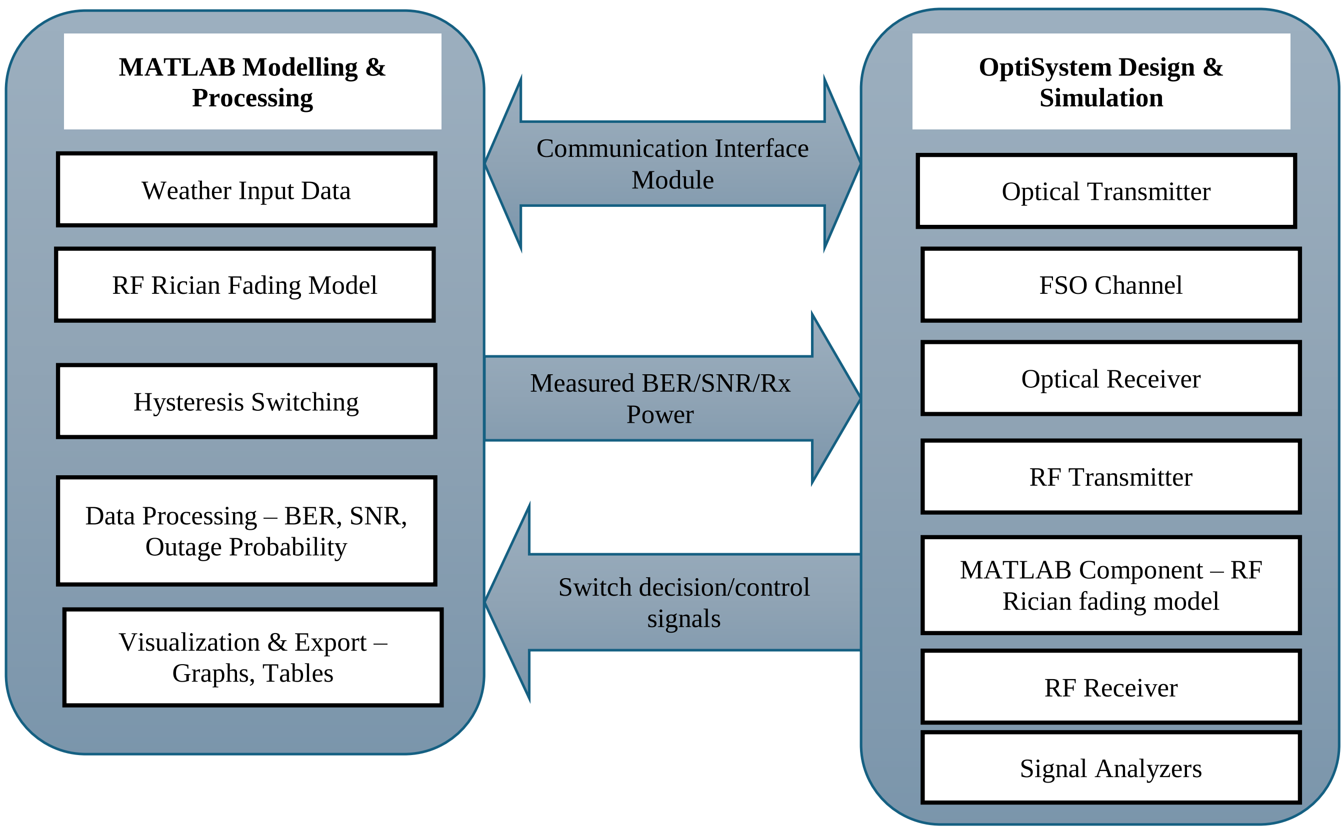

Fig. 2 OptiSystem-MATLAB Co-simulation framework

4. Performance Analysis

The performance analysis makes a comparison between an independent system-level simulation done in OptiSystem and MATLAB, and a numerical evaluation of the theoretical model done in MATLAB, enabling both analytical insight and practical validation of this work.

4.1. Outage probability of the FSO link

Outage probability is defined as the probability that the received average SNR is below a given minimum SNR threshold. The SNR threshold value is established by identifying the operating point at which the received signal quality degrades beyond an acceptable limit. In this work, the target quality-of-service requirement for the FSO link is specified in terms of a target Bit Error Rate (BER) of $P_e^* = 10^{-6}$.

The SNR threshold is obtained numerically from the simulated BER and SNR characteristics of the system under varying atmospheric conditions. Specifically, the threshold SNR, denoted by $\gamma_{\text{thr, FSO}}$, is interpreted as the SNR value corresponding to the point at which the simulated BER curve intersects the target BER level for the FSO link. This can be expressed as

$$P_{out} = Pr(P_e > P^*{}_e) \equiv P(\gamma_{FSO} < \gamma_{thrFSO}{}^*) \quad (12)$$

Where γ_{FSO} denotes the effective electrical SNR at the receiver, and $\gamma_{thr\ FSO}{}^*$ is the numerically extracted SNR threshold corresponding to P_e^*.

For a specific channel realization h, the error probability conditioned on that instantaneous channel state is expressed as

$$P_{CEP}(h) = \frac{1}{2}\left(erfc\sqrt{\frac{\gamma(h)}{2}}\right) \quad (13)$$

Where, γ(h) is the instantaneous electrical SNR associated with the channel realization h.

For each weather condition, the Gamma-Gamma channel model is sampled across a large ensemble of independent realizations. The instantaneous SNR and BER are computed for each trial, from which the outage probability is estimated by counting the fraction of realizations that fail to meet the target threshold.
The FSO outage probability is then estimated as

$$P_{\text{out,FSO}} \approx \frac{1}{N_{\text{MC}}} \sum_{k=1}^{N_{\text{MC}}} \mathbb{I}\left[\gamma_{FSO} < \gamma_{thrFSO}\right] \quad (14)$$

Where N_{MC} is the number of Monte-Carlo realizations, γ_{FSO} is the effective SNR for the k-th realization, and $\mathbb{I}[\cdot]$ is the indicator function.

Based on this instantaneous SNR, the instantaneous Bit Error Rate (BER) is evaluated as $P_{b,inst} = Q(\sqrt{\gamma_{FSO}})$

4.2. Outage probability of the RF link

For the RF link, outage probability is defined using the same fundamental criterion as the FSO link, namely, the probability that the received signal quality lies below a predetermined threshold. The RF link in the proposed hybrid architecture serves primarily as a backup link to guarantee connectivity during adverse weather conditions. The quality-of-service requirement for the RF link is thus also specified in terms of a BER target of 10^{-6}. The SNR threshold that meets this target BER is also obtained numerically from the BER-SNR curves under the prevailing weather conditions. Accordingly, the RF outage probability is defined as

$$P_{out} = Pr(\gamma_{RF} < \gamma_{thr,RF})$$

For the RF link, the instantaneous SNR is expressed as

$$\gamma_{RF} = \frac{P_{rx}|h|^2}{P_{noise}} \quad (15)$$

where h denotes the small-scale Rician fading coefficient, P_{rx} is the average received RF power including path loss, attenuation due to rain, oxygen and fog, and P_{noise} represents the total receiver noise power.

The outage behavior is evaluated numerically using Monte-Carlo simulations by averaging the number of realizations for which the instantaneous SNR falls below the threshold.

Based on this instantaneous SNR, the instantaneous Bit Error Rate (BER) is evaluated as

$$P_{b,inst} = \frac{4}{log_2 M}\left(1 - \frac{1}{\sqrt{M}}\right) Q\left(\sqrt{\frac{3log_2 M}{M-1}\,\gamma_{RF}}\right) \quad (16)$$

4.3. Outage Probability of the Hybrid System

When the SNR of both the FSO and RF link is below the respective thresholds for each of the systems, then the system will be in outage. The outage probability of the hybrid FSO-RF system is given by

$$P_{out,hyb} = P_{out,FSO} \times P_{out,RF} \quad (17)$$

5. Results and Discussion

For the investigation of the influence of fog-induced degradation in FSO and RF systems, the visibility values vary from 0.01 to 1 km. In the visibility range of 0.01-0.2 km, the atmospheric conditions correspond to dense to light fog. To evaluate the impact of fog on the mm wave RF link within this visibility range, the ITU-R P.840-7 guideline is used.

The simulated BER and SNR values are captured in the BER Analyzer and Electrical Carrier Analyzer (ECAN), respectively. Cross-validation against the analytical expressions derived in Section 3 confirms the accuracy of the simulation framework across the tested visibility range.

As visibility decreases, the FSO link experiences a rapid degradation in performance, while the RF SNR varies by less than 3 dB over the same range, as Figures 4 and 5 confirm, respectively.

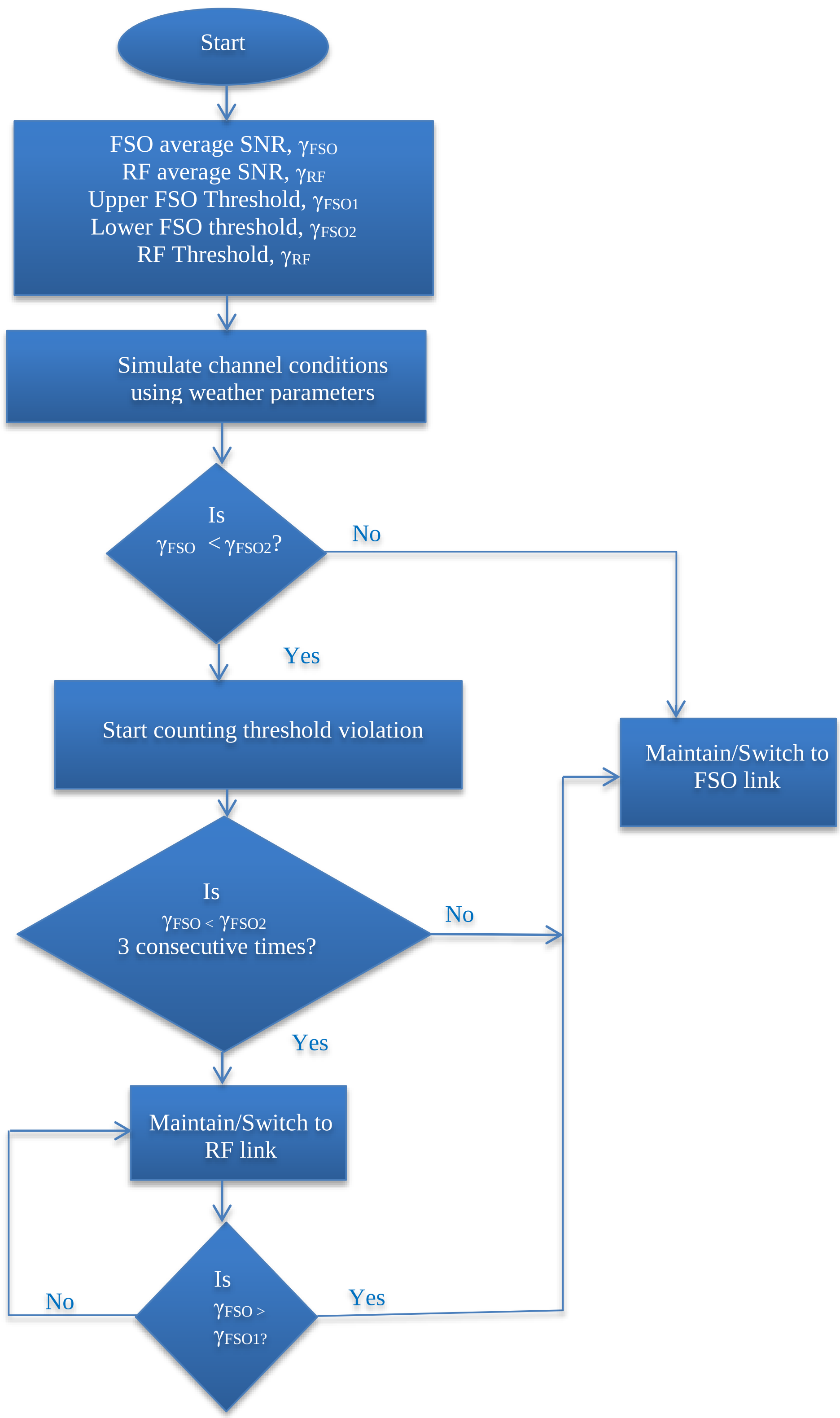

Fig. 3 Flowchart illustrating the hysteresis-based switching mechanism of the hybrid FSO-RF system

The increase in BER for the FSO link is primarily due to Mie scattering caused by fog particles with sizes comparable to the optical wavelength. In contrast, the RF link maintains low BER across the evaluated visibility conditions, making it suitable as a backup link during periods of reduced visibility.

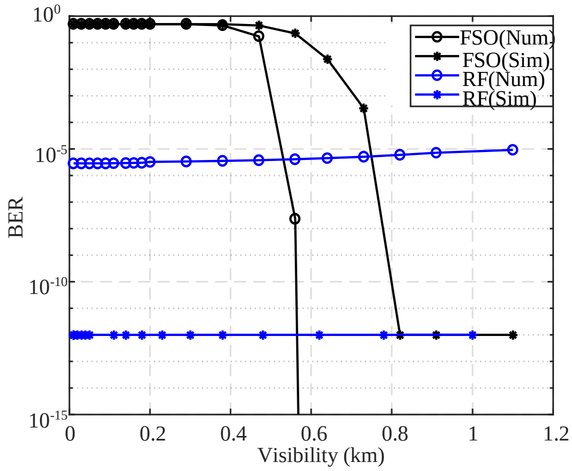

Fig. 4 Average Bit Error Rate (BER) of the FSO and RF links as a function of atmospheric visibility in the fog-dominated regime (visibility ≤ 1.1 km). Numerical results (Num) are obtained from analytical BER expressions using the average received SNR, while Simulation results (Sim) reflect system-level simulations under quasi-static channel conditions

Using a BER target of 10^{-6}, the FSO operating limit under fog is identified at a visibility of 0.76 km. Mapping this point to the corresponding SNR curve in Figure 5 yields an FSO switching threshold of 12.72 dB, which is used as the lower FSO SNR threshold value in the developed model for switching.

The RF SNR for the numerical and simulation results remain largely invariant with visibility as presented in Figure 5, as fog-induced attenuation has a negligible impact at mm Wave frequencies compared to optical wavelengths.

A consistent offset can be seen between the numerical and simulated RF SNR results, with the simulated values appearing generally higher. The observed offset arises from the difference in noise power normalization and averaging procedures.

The numerical RF SNR provides a conservative, propagation-level estimate based on fixed noise bandwidth assumptions. In contrast, the simulated SNR is obtained from finite-length waveform realizations corresponding to specific channel instances. The numerical FSO SNR represents an idealized channel-level metric derived under simplified receiver assumptions.

The simulated FSO SNR is measured at the receiver front end after the propagation channel and EDFA amplification stage. As a result, the measured values include receiver-side effects such as finite optical bandwidth, gain normalization, and practical noise contributions that are not included in the analytical model. At high levels of visibility, the simulated FSO SNR reaches a bounded level, while the numerical SNR continues to increase under idealized assumptions.

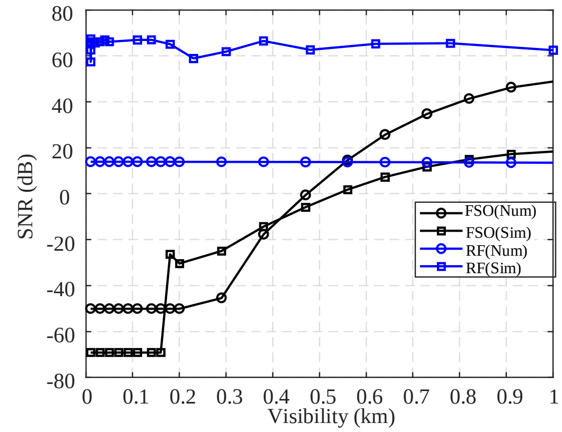

Fig. 5 Average Signal-to-Noise Ratio (SNR) of the FSO and RF links as a function of atmospheric visibility. Numerical results (Num) are obtained from analytical SNR expressions, while Simulation results (Sim) reflect system-level simulations under quasi-static channel conditions

Although the absolute values differ, both numerical and simulated results follow the same trend with changing visibility, showing a clear improvement in SNR as atmospheric attenuation decreases. For the RF link, fog produces only minor attenuation at mmWave frequencies; therefore, the SNR threshold cannot be identified from the fog analysis presented in Figures 4 and 5. For this reason, rainfall is used to evaluate the RF link performance and determine the corresponding threshold SNR. For this, the rainfall rate is varied from 0 – 100 mm/hr.

Figure 6 shows the SNR comparison, while Figure 7 shows the BER comparison of the two links as a function of rainfall. Both links experience performance degradation; however, the RF link exhibits a significantly steeper reduction in its SNR compared to the FSO link. This behavior is consistent with the heavy rain absorption and scattering effects at mm.

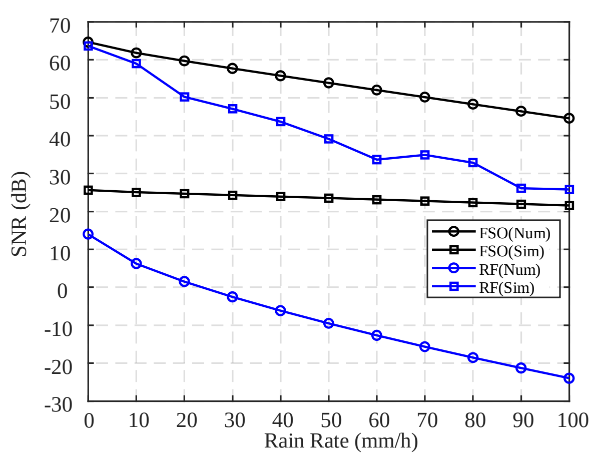

Fig. 6 Average Signal-to-Noise Ratio (SNR) of the FSO and RF links as a function of atmospheric rainfall rate. Numerical results are obtained from analytical SNR expressions, while simulation results reflect system-level simulations under quasi-static channel conditions

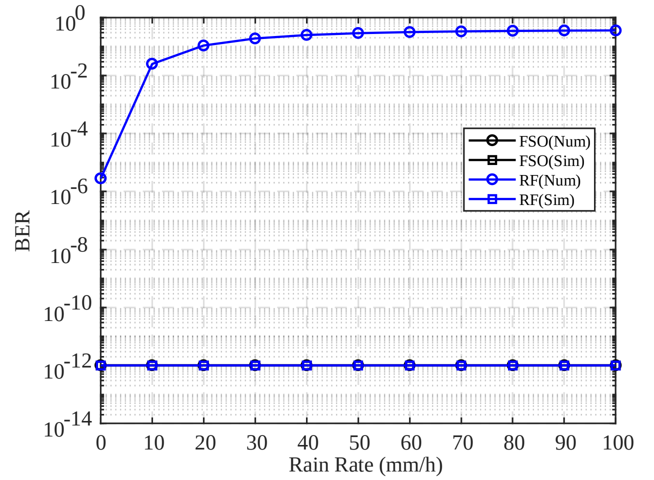

Fig. 7 Average Bit Error Rate (BER) of the FSO and RF links as a function of atmospheric rainfall. Numerical results (Num) are obtained from analytical BER expressions using the average received SNR, while Simulation results (Sim) reflect system-level simulations under quasi-static channel conditions

Wave frequencies, whereas the optical FSO link is comparatively less sensitive to rainfall-induced attenuation.

Despite this degradation, the RF link maintains a BER well below the BER target of 10^{-6} over the rainfall range, as presented in Figure 7, confirming its suitability as a reliable backup for the FSO link.

The RF SNR threshold is thus based on equation 16, which gives 14dB. The 16-QAM mm Wave RF demonstrates robust operation under heavy rainfall conditions up to 100mm/h, highlighting the effectiveness of the proposed switching strategy in mitigating weather-induced outages. The numerical RF BER represents a conservative estimate based on propagation-level SNR assumptions, whereas the simulated RF BER is measured after receiver-side processing, including matched filtering and effective noise bandwidth reduction. For the chosen system parameters, the post-detection SNR remains sufficiently high to yield error-free reception within the finite simulation sequence length, resulting in a near-zero BER floor.

Outage behavior with varying visibility across all three configurations - FSO-only, RF-only and the hybrid system is presented in Figure 8, while Figure 9 shows the outage behavior over the same rainfall rate. In Figure 8, for visibility below 0.76 km, the hybrid system maintains connectivity. While the FSO link experiences severe degradation, the RF backup link maintains connectivity, thereby preserving overall link availability.

In Figure 9, both links maintain SNR values above their required thresholds over the evaluated rainfall range. Under these conditions, no outage is observed in the hybrid FSO-RF system.

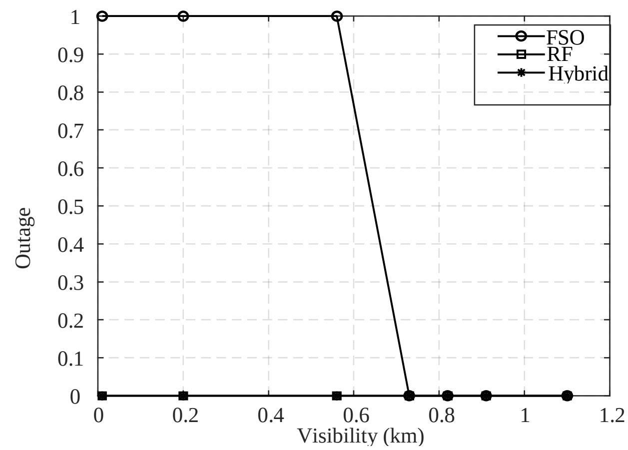

Fig. 8 Outage probability comparison of the FSO-only, RF-only and hybrid FSO-RF system in the fog-dominated regime (visibility ≤ 1.1 km). The results captured reflect system-level simulations under quasi-static channel conditions

Tables 4 and 5 summarize the operation of the switching mechanism under varying atmospheric conditions. At each iteration, the average SNR values of both links are checked against the predefined switching thresholds to select the active transmission link. A persistence hold of three consecutive below-threshold observations is used before switching is initiated. This reduces unnecessary switching caused by short-term fluctuations. While increasing the persistence (hold) duration can further reduce the number of switching events, it also introduces a trade-off, as delayed switching may lead to increased outage under severe channel degradation. The system-level simulation adopts a quasi-static channel model, whereby each simulation iteration corresponds to a fixed atmospheric condition. Consequently, switching decisions are made across successive simulation runs rather than during a single simulation window. The SNR values obtained in Tables 4 and 5 are used to compare the performance of the proposed hysteresis-based switching against alternative switching methods.

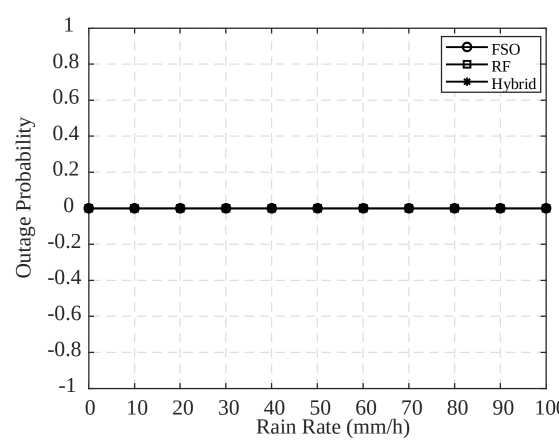

Fig. 9 Outage probability of the FSO, RF and hybrid FSO-RF system comparison as a function of atmospheric rainfall rate. The results captured reflect system-level simulations under quasi-static channel conditions

In this analysis, the time-series simulation reflects the behavior of the switching logic and controller memory, without modeling fast channel variations, as demonstrated in Figure 10. The outage probability is then computed as the decision intervals during which the active link fails to satisfy the target SNR requirement. For comparison, the Fuzzy Inference System (FIS) used in [6] is modeled.

Table 4. Hysteresis-based switching with varying atmospheric visibility conditions

Iter.	Visibility (km)	FSO SNR (dB)	RF SNR (dB)	Link Before	Link After
1	1.1	17.26	58.52	FSO	FSO
2	0.91	16.81	64.00	FSO	FSO
3	0.82	16.09	65.09	FSO	FSO
4	0.2	-63.06	66.76	FSO	FSO
5	0.2	-33.57	68.25	FSO	FSO
6	0.56	7.00	67.10	FSO	RF
7	0.91	16.80	66.38	RF	RF
8	1.1	17.29	66.87	RF	RF
9	1.1	17.30	57.83	RF	FSO

Each visibility condition was evaluated over 100 decision intervals, using a persistence hold of three consecutive below-threshold observations. For visibility values at which the FSO outage fraction was greater than zero, the percentage reduction achieved by the proposed scheme was calculated as

$$R(V) = \frac{P_{out-frac,FSO}(V) - P_{out-frac,prop}(V)}{P_{out-frac,FSO}(V)} * 100\%. \quad (18)$$

For example, at V= 0.64 km: the FSO-only outage fraction ($P_{out-frac,FSO}$) was 1, whereas the proposed hysteresis outage fraction ($P_{out-frac,prop}$) was 0.02. The corresponding reduction in this visibility was therefore 98%. The overall reduction was calculated by pooling the outage fractions across all evaluated visibility conditions:

$$R_{overall} = \frac{\sum_i P_{out-frac,FSO}(V_i) - \sum_i P_{out-frac,prop}(V_i)}{\sum_i P_{out-frac,FSO}(V_i)} * 100\% \quad (19)$$

The mean outage fraction for the FSO-only link is 0.5294 and 0.0027 for the proposed scheme gives an overall reduction of approximately 99.49%.

The time-series simulation results reveal distinct behaviors across the switching strategies. Figure 11 captures the switching activity of the links. The performance of the proposed hysteresis-based switching strategy demonstrates significant improvement over benchmark strategies evaluated, specifically single-threshold hard switching and Fuzzy Inference System (FIS)-based switching. The improved performance of the proposed framework is mainly due to the use of persistence hold together with post-detection SNR thresholding. Conventional single-threshold hard switching relies on instantaneous channel evaluations to make link transitions. Although this method can maintain a low outage probability, it is highly sensitive to rapid short-term signal variations. This can trigger unnecessary link transitions, which can degrade overall data throughput and system stability. By implementing persistence-hold, the proposed strategy reduces unnecessary switching events by 22% relative to the single threshold approach while maintaining an identical, near-zero outage probability. The proposed method shows better link reliability than the FIS-based switching approach. The FIS method relies primarily on atmospheric visibility rather than instantaneous link quality to dictate switching decisions. As a result, it can fail to react to localized, severe signal degradation, causing the system to remain on a degraded FSO link, resulting in a higher outage probability. In contrast, the proposed strategy utilizes direct measurements of the electrical SNR at the receiver front-end. This ensures the system transitions to the mm-wave RF backup when the optical signal integrity is compromised, achieving a superior balance between switching stability and continuous link availability.

Table 5. Hysteresis-based switching with varying atmospheric rainfall conditions

Iter.	Rainfall (mm/h)	SNR FSO (dB)	SNR RF (dB)	Link Before	Link After
1	0	17.73	58.52	FSO	FSO
2	10	17.70	56.13	FSO	FSO
3	15	17.67	54.64	FSO	FSO
4	25	17.66	51.72	FSO	FSO
5	75	17.40	36.66	FSO	FSO
6	100	17.24	28.77	FSO	FSO
7	50	17.51	42.74	FSO	FSO
8	25	17.64	52.29	FSO	FSO
9	10	17.66	50.07	FSO	FSO
10	15	17.66	57.52	FSO	FSO
11	20	17.64	53.04	FSO	FSO

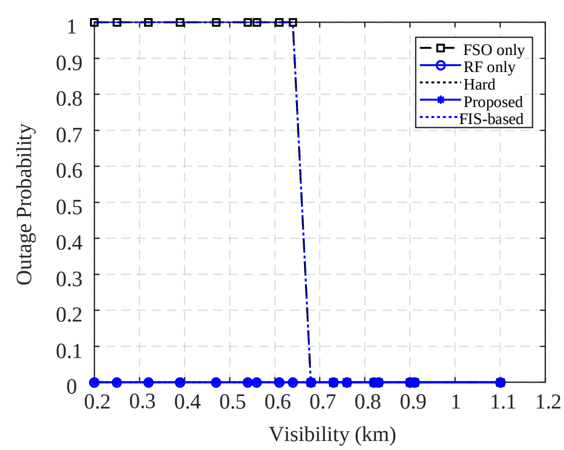

Fig. 10 Time-series outage probability comparison for FSO-only, RF-only, single-threshold hard switching, FIS-based switching, and the proposed hysteresis-based switching mechanism under varying visibility conditions. Time-series simulation shows the switching logic and controller memory

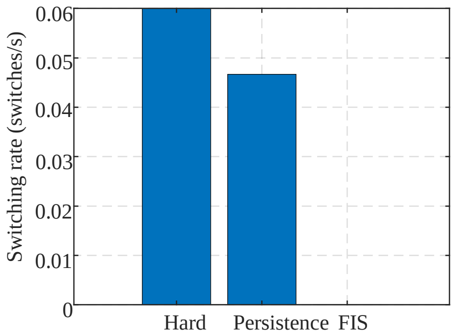

Fig. 11 Switching Rate Comparison as a function of atmospheric visibility of Single threshold hard-switching mechanism, FIS-based Switching mechanism and the proposed hysteresis-based switching mechanism

6. Conclusion

A hysteresis-based hard-switching mechanism for a hybrid FSO-RF system was evaluated under atmospheric turbulence, fog, and rain-induced atmospheric impairments. The analysis used fixed switching thresholds of 12.72 dB for the FSO link and 14 dB for the RF link. For these threshold values, the hybrid system maintained an outage probability below 10^{-4} under all evaluated weather conditions. Compared with the FSO-only link, the proposed mechanism achieved an overall reduction of 99.49% in the outage fraction across the evaluated visibility conditions. It also reduced unnecessary switching events by 22% while preserving low outage probability relative to a single-threshold scheme.

The OptiSystem-MATLAB co-simulation framework provides a practical method for assessing link availability and switching behavior in hybrid FSO-RF systems under quasi-static channel conditions. The same framework may be extended to include time-varying channel models, adaptive thresholds and intelligent switching mechanisms. Future work will extend the framework to adaptive and learning-based switching methods, including deep reinforcement learning for dynamic switching under time-varying channel conditions.

Conflicts of Interest

The authors declare that there is no conflict of interest regarding the publication of this paper.

Funding Statement

This work was supported by the African Union Commission under the Pan-African University scholarship.

References

[1] Mosa Ali Abu-Rgheff, *5G Physical Layer Technologies*, Wiley, 2019. [CrossRef] [Google Scholar] [Publisher Link]

[2] Anthony Ngozichukwuka Uwaechi, and Nor Muzlifah Mahyuddin, "A Comprehensive Survey on Millimeter Wave Communications for Fifth-Generation Wireless Networks: Feasibility and Challenges," *IEEE Access*, vol. 8, pp. 62367-62414, 2020. [CrossRef] [Google Scholar] [Publisher Link]

[3] Ch V. V. S. Sriniva, and Somasekhar Borugadda, "RF Chain Selection Using Hybrid Optimization with Precoding in mm-Wave Massive MIMO Systems," *Wireless Personal Communications*, vol. 131, no. 3, pp. 1997-2017, 2023. [CrossRef] [Google Scholar] [Publisher Link]

[4] Mostafa Zaman Chowdhury et al., "Optical Wireless Hybrid Networks: Trends, Opportunities, Challenges, and Research Directions," *IEEE Communications Surveys and Tutorials*, vol. 22, no. 2, pp. 930-966, 2020. [CrossRef] [Google Scholar] [Publisher Link]

[5] Wenzhe Zhang, Steve Hranilovic, and Ce Shi, "Soft-Switching Hybrid FSO/RF Links Using Short-Length Raptor Codes: Design and Implementation," *IEEE Journal on Selected Areas in Communications*, vol. 27, no. 9, pp. 1698-1708, 2009. [CrossRef] [Google Scholar] [Publisher Link]

[6] Abid Ali Minhas et al., "Attenuation-based Hybrid RF/FSO Link using Soft Switching," *Optical Engineering*, vol. 60, no. 5, pp. 1-22, 2021. [CrossRef] [Google Scholar] [Publisher Link]

[7] Sarma Vangala, and Hossein Pishro-Nik, "A Highly Reliable FSO/RF Communication System Using Efficient Codes," *IEEE GLOBECOM 2007 - IEEE Global Telecommunications Conference*, Washington, DC, USA, pp. 2232-2236, 2007. [CrossRef] [Google Scholar] [Publisher Link]

[8] Matúš Tatarko, Ľuboš Ovseník, Ján Turán, "Switching of Hybrid FSO/RF Link Using Fog Sensor," *Carpathian Journal of Electronic and Computer Engineering*, vol. 7, no. 2, pp. 11-14, 2014. [Google Scholar] [Publisher Link]

[9] Muneer Usman, Hong-Chuan Yang, and Mohamed-Slim Alouini, "Practical Switching-Based Hybrid FSO/RF Transmission and Its Performance Analysis," *IEEE Photonics Journal*, vol. 6, no. 5, pp. 1-13, 2014. [CrossRef] [Google Scholar] [Publisher Link]

[10] Mojtaba Mansour Abadi et al., "Hard Switching in Hybrid FSO/RF Link: Investigating Data Rate and Link Availability," *2017 IEEE International Conference on Communications Workshops, ICC Workshops 2017*, Paris, France, pp. 463-468, 2017. [CrossRef] [Google Scholar] [Publisher Link]

[11] Abdullateef Almohamad et al., "Enhancing Performance in Hybrid RF/FSO Systems: Leveraging Level Crossing Rate for Seamless Switching," *2023 IEEE International Black Sea Conference on Communications and Networking (BlackSeaCom)*, Istanbul, Turkiye, pp. 289-293, 2023. [CrossRef] [Google Scholar] [Publisher Link]

[12] Shreesh Kumar Shrivastava et al., "Threshold Optimization for Modified Switching Scheme of Hybrid FSO/RF System in the Presence of Strong Atmospheric Turbulence," *Photonic Network Communications*, vol. 40, no. 2, pp. 103-113, 2020. [CrossRef] [Google Scholar] [Publisher Link]
[13] Banibrata Bag et al., "Performance Analysis of Hybrid FSO Systems Using FSO/RF-FSO Link Adaptation," *IEEE Photonics Journal*, vol. 10, no. 3, pp. 1-17, 2018. [CrossRef] [Google Scholar] [Publisher Link]
[14] Hasan Tahsin Toplar, and Murat Uysal, "Modeling of Pointing Errors in Terrestrial FSO Links Caused by Building Sway Under Wind Loads," *IEEE Open Journal of the Communications Society*, vol. 6, pp. 1161-1169, 2025. [CrossRef] [Google Scholar] [Publisher Link]
[15] Negin Nikbakht-Sardari et al., "Novel Adaptive Hard-Switching based Hybrid RF-FSO System Architecture using Two Threshold Values in the Presence of Atmospheric Turbulence and Pointing Error," *Results in Engineering*, vol. 17, pp. 1-8, 2023. [CrossRef] [Google Scholar] [Publisher Link]
[16] Maroš Lapčák et al., "Investigation of Machine Learning Methods for Prediction of Measured Values of Atmospheric Channel for Hybrid FSO/RF System," *Photonics*, vol. 9, no. 8, pp. 1-18, 2022. [CrossRef] [Google Scholar] [Publisher Link]
[17] Maroš Lapčák et al., "Deep Data Analysis Methods Applied to Hard Switching in Hybrid FSO/RF Systems," *2023 33rd International Conference Radioelektronika, RADIOELEKTRONIKA 2023*, Pardubice, Czech Republic, pp. 1-6, 2023. [CrossRef] [Google Scholar] [Publisher Link]
[18] Song Song et al., "Hybrid FSO/RF System Using Intelligent Power Control and Link Switching," *IEEE Photonics Technology Letters*, vol. 33, no. 18, pp. 1018-1021, 2021. [CrossRef] [Google Scholar] [Publisher Link]
[19] Song Song et al., "Channel Prediction for Intelligent FSO Transmission System," *Optics Express*, vol. 29, no. 17, pp. 27882-27889, 2021. [CrossRef] [Google Scholar] [Publisher Link]
[20] Song Song et al., "Demonstration of Intelligent Hybrid FSO/RF System Based on Enhanced GRU Prediction and Real-World Meteorological Dataset," *Journal of Lightwave Technology*, vol. 40, no. 21, pp. 7048-7059, 2022. [CrossRef] [Google Scholar] [Publisher Link]
[21] Kritica Sharma, Sanmukh Kaur, and Hardeep Singh, "Channel Modelling and Performance Analysis of Switching based Hybrid FSO/RF Communication System," *Journal of Optics*, 2025. [CrossRef] [Google Scholar] [Publisher Link]
[22] Somia A. Abd El-Mottaleb et al., "Harnessing the Power of ML for Robust SISO and MIMO FSO Communication Systems in fog Weather," *Optical and Quantum Electronics*, vol. 56, no. 6, pp. 1-17, 2024. [CrossRef] [Google Scholar] [Publisher Link]
[23] Han Zeng et al., "Enhancing Robustness in Hybrid FSO/RF Systems: A Feedback-Free Approach Leveraging Deep Learning for Real-Time Power Allocation," *IEEE Internet of Things Journal*, vol. 12, no. 13, pp. 24358-24373, 2025. [CrossRef] [Google Scholar] [Publisher Link]
[24] Junhu Shao et al., "Adaptive Modulation Scheme for Soft-Switching Hybrid FSO/RF Links Based on Machine Learning," *Photonics*, vol. 11, no. 5, pp. 1-13, 2024. [CrossRef] [Google Scholar] [Publisher Link]
[25] Shagufta Henna et al., "Ensemble Consensus Representation Deep Reinforcement Learning for Hybrid FSO/RF Communication Systems," *Optics Communications*, vol. 530, pp. 1-13, 2023. [CrossRef] [Google Scholar] [Publisher Link]
[26] Maged Abdullah Esmail, Habib Fathallah, and Mohamed-Slim Alouini, "Analysis of Fog Effects on Terrestrial Free Space Optical Communication Links," *2016 IEEE International Conference on Communications Workshops (ICC)*, Kuala Lumpur, Malaysia, pp. 151-156, 2016. [CrossRef] [Google Scholar] [Publisher Link]
[27] M. S. Awan et al., "Cloud Attenuations for Free-Space Optical Links," *2009 International Workshop on Satellite and Space Communications*, Siena, Italy, pp. 274-278, 2009. [CrossRef] [Google Scholar] [Publisher Link]
[28] A.Z. Suriza et al., "Proposed Parameters of Specific Rain Attenuation Prediction for Free Space Optics Link Operating in Tropical Region," *Journal of Atmospheric and Solar-Terrestrial Physics*, vol. 94, pp. 93-99, 2013. [CrossRef] [Google Scholar] [Publisher Link]
[29] Abir Touati et al., "On the Effects of Combined Atmospheric Fading and Misalignment on the Hybrid FSO/RF Transmission," *Journal of Optical Communications and Networking*, vol. 8, no. 10, pp. 715-725, 2016. [CrossRef] [Google Scholar] [Publisher Link]